

NASA Technical Memorandum 4526

Reduction of Structural Loads Using Maneuver Load Control on the Advanced Fighter Technology Integration (AFTI)/F-111 Mission Adaptive Wing

Stephen V. Thornton

September 1993



EXACT COPY

FOR DISTRIBUTION

DO NOT REPRODUCE THIS FROM

Reduction of Structural Loads Using Maneuver Load Control on the Advanced Fighter Technology Integration (AFTI)/F-111 Mission Adaptive Wing

Stephen V. Thornton
*Dryden Flight Research Facility
Edwards, California*



National Aeronautics and
Space Administration
Office of Management
Scientific and Technical
Information Program

1993

CONTENTS

ABSTRACT	1
NOMENCLATURE	1
INTRODUCTION	2
AIRCRAFT DESCRIPTION	4
INSTRUMENTATION	7
FLIGHT TEST CONDITIONS	10
RESULTS AND DISCUSSION	11
Wing-Root Loads12
Wing-Box Loads17
High-Camber Configurations20
Forward Spar Web Shear21
Stabilator Pitch Trim Loads21
Automatic Modes23
CONCLUDING REMARKS	27
REFERENCES	28

ABSTRACT

A transonic fighter-bomber aircraft, having a swept supercritical wing with smooth variable-camber flaps was fitted with a maneuver load control (MLC) system that implements a technique to reduce the inboard bending moments in the wing by shifting the spanwise load distribution inboard as load factor increases. The technique modifies the spanwise camber distribution by automatically commanding flap position as a function of flap position, true airspeed, Mach number, dynamic pressure, normal acceleration, and wing sweep position. Flight test structural loads data were obtained for loads in both the wing box and the wing root. Data from uniformly deflected flaps were compared with data from flaps in the MLC configuration where the outboard segment of three flap segments was deflected downward less than the two inboard segments. The changes in the shear loads in the forward wing spar and at the roots of the stabilators also are presented. The camber control system automatically reconfigures the flaps through varied flight conditions. Configurations having both moderate and full trailing-edge flap deflection were tested. Flight test data were collected at Mach numbers of 0.6, 0.7, 0.8, and 0.9 and dynamic pressures of 300, 450, 600, and 800 lb/ft². The Reynolds numbers for these flight conditions ranged from 26×10^6 to 54×10^6 at the mean aerodynamic chord. Load factor increases of up to 1.0 g were achieved with no increase in wing-root bending moment with the MLC flap configuration.

NOMENCLATURE

Physical quantities in this report are given in the U.S. customary system of units. Reference 1 gives the factors for conversion to the international system of units.

AFTI	advanced fighter technology integration
B	wing-root bending moment, in-lb
C_D	coefficient of drag
CCC	cruise camber control
c.g.	aircraft center of gravity location, in.
C_L	coefficient of lift
g	gravitational constant, 32.2 ft/sec ²
g_e	equivalent load factor = $\frac{\text{maneuver gross weight} \times \text{load factor}}{\text{design gross weight (70,000 lb)}}$
L/D	lift-to-drag ratio, (C_L / C_D)
M	Mach number
MAC	mean aerodynamic chord
MAW	mission adaptive wing
MEGA	maneuver enhancement/gust alleviation
MCC	maneuver camber control
MLC	maneuver load control
n_z	normal acceleration, g

\bar{q}	free-stream dynamic pressure, lb/ft ²
T	wing-root torsion, in-lb
TACT	transonic aircraft technology
W	aircraft gross weight, lb
α	aircraft angle of attack, deg
δ_h	pitch stabilator deflection; trailing edge down is positive (average of left and right stabilator deflections), deg
δ_{LE}	deflection of the leading-edge flap; down is positive, deg
δ_{TE}	deflection of the midspan and inboard trailing-edge flaps; down is positive, deg
δ_{TEO}	deflection of the outboard trailing-edge flap; down is positive, deg

INTRODUCTION

Designers of modern high-performance aircraft usually employ electronic automatic control systems either to augment the mechanical control systems or to implement a set of complex control laws. Such control laws often are required to maximize the performance of an aircraft with multiple advanced aerodynamic control surfaces or to give acceptable handling qualities to an aircraft having relaxed static stability. Such a control system provides an excellent opportunity to implement structural load-relieving modes in combination with the basic control system. The advanced fighter technology integration (AFTI)/F-111 aircraft has such a control system. Figure 1 shows the test aircraft in flight with flaps deflected. The AFTI/F-111 flight test program was accomplished by the NASA Dryden Flight Research Facility with the assistance of the Air Force Flight Test Center, Edwards AFB, California. The program investigated the characteristics of performance-enhancing automatic controls as described in more detail in reference 2.

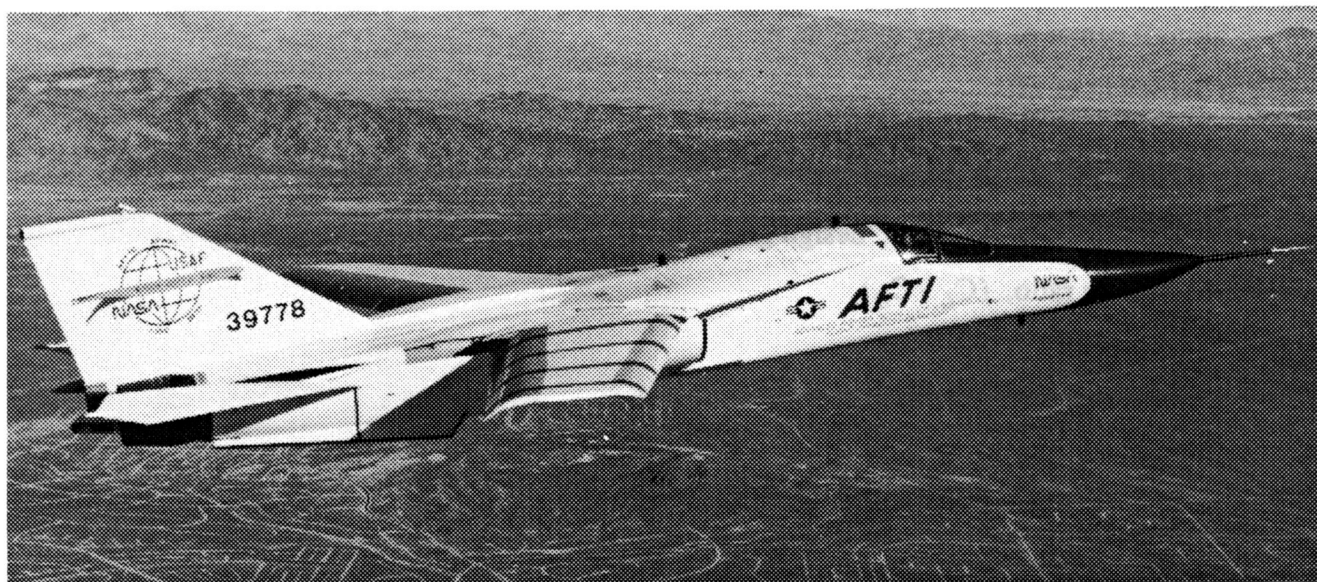


Figure 1. The AFTI/F-111 in flight with flaps deflected.

EC86-3385-002

The AFTI/F-111 modification included the design and installation of four automatic control modes: (1) cruise camber control (CCC), (2) maneuver camber control (MCC), (3) maneuver enhancement/gust alleviation (MEGA), and (4) maneuver load control (MLC) (ref. 2). The CCC mode seeks to maximize the cruise speed of the aircraft for a given fixed throttle setting by making small, iterative changes in flap settings and waiting to evaluate the effect on velocity. The CCC mode was designed to be used by itself. The MCC mode attempts to maximize the maneuvering lift-to-drag ratio (L/D) of the aircraft by increasing camber with increasing load factor according to a predetermined flap schedule (derived from wind-tunnel data) in the control system. The MLC mode redistributes the aerodynamic load over the wingspan by modifying the local camber of the airfoil using variable flap positions to reduce the wing-root bending moment. The MEGA mode responds only to normal force transients either by rapidly adding camber to the wing to enhance the load factor control response of the aircraft or by reducing the wing camber to attenuate the gust response of the aircraft. The MCC, MEGA, and MLC modes could be activated either individually or in any combination. The MLC mode, which is also the subject of the author's paper in reference 3, will be discussed here in greater detail. Limited data also are presented for the combined MCC and MLC modes. The design, purpose, and performance of the other modes are discussed at greater length in reference 4.

Maneuver load control, sometimes called "maneuver load alleviation," is the technique of changing the lift distribution along the span of the wing to move the center of lift inboard, thus reducing the wing bending moments. The technique is achieved by automatically changing either the wing twist or the wing camber distribution along the span or both, usually by deflecting appropriate flaps. Several studies have been conducted on the subject; some of which have been reported in references 5 through 8. The aircraft referred to in the references, however, did not have a smooth variable-camber wing. Therefore, the AFTI/F-111 aircraft provided the first opportunity to conduct MLC experiments on an aircraft of this size (83,000 lb gross weight (W)) with a wing loading of approximately 133 lb/ft^2 , speed (high subsonic range), and Reynolds number (26×10^6 to 54×10^6 at the mean aerodynamic chord (MAC) of 131.36 in.), which also had a smooth variable-camber wing.

The prime objective of this work, which used the smooth variable-camber wing of the AFTI/F-111 with its multisegmented trailing-edge flaps, was to quantify the effects of Mach number (M), dynamic pressure (\bar{q}), and MLC flap configuration changes upon wing-root bending moment and other aircraft structural loads. Evaluations are made regarding the pitch trim load changes on the stabilator caused by MLC flap configuration changes. Observations also are made regarding the effects of MLC pitch trim loads upon aircraft performance for selected maneuvers. Aircraft component loads at different combinations of leading and trailing-edge flap positions are compared with two baseline flap configurations at several Mach numbers and dynamic pressures. The term "baseline" designates either of two flap configurations chosen for discussion having uniform trailing-edge deflections (δ_{TE}) with which variations in outboard trailing-edge deflections (δ_{TEO}) are compared.

Figure 2 illustrates the effect of MLC on the spanwise lift distribution. Figure 2(a) shows an approximate spanwise load distribution for a wing having uniform trailing-edge flap deflections with the area under the distribution curve representing total lift. Figure 2(b) illustrates the MLC effect in which a total lift equal to that shown in fig. 2(a) is produced by raising the outboard segment of the trailing-edge flap to its full up (approximately -1°) position, while the deflection of the midspan and inboard segments are increased slightly to offset the reduced lift from the outboard portion of the wing. A comparison of figures 2(a) and 2(b) shows that an equal total lift centered closer to the wing root produces less bending moment.

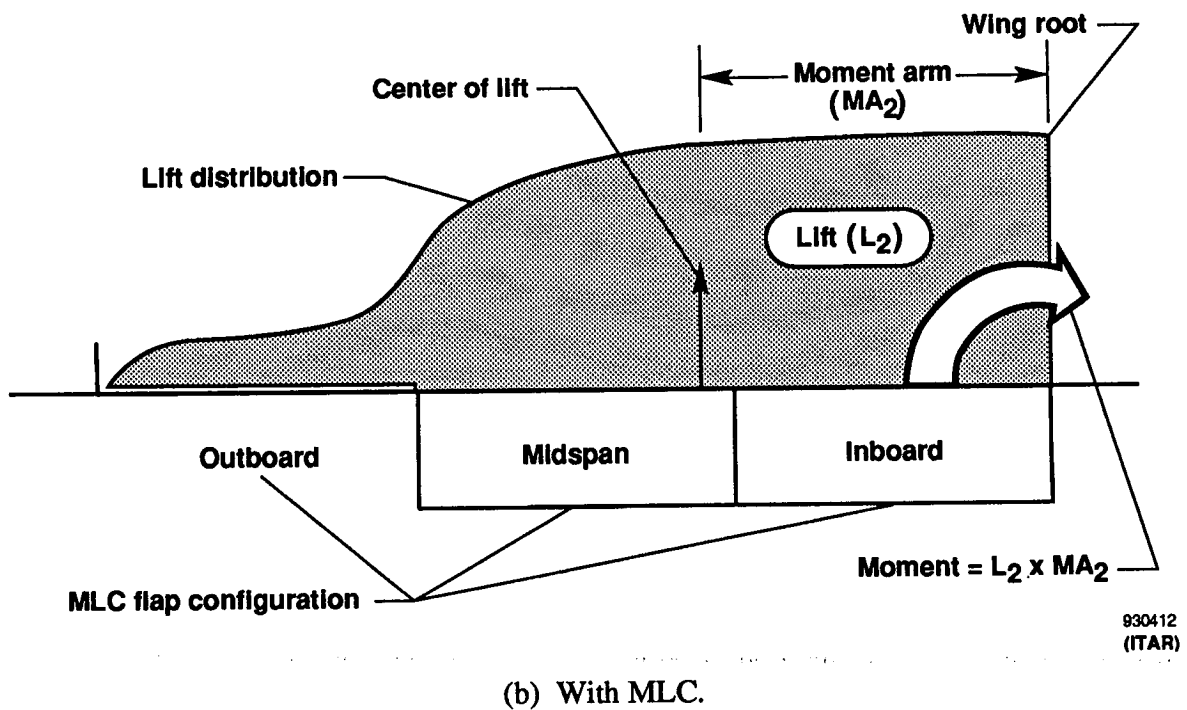
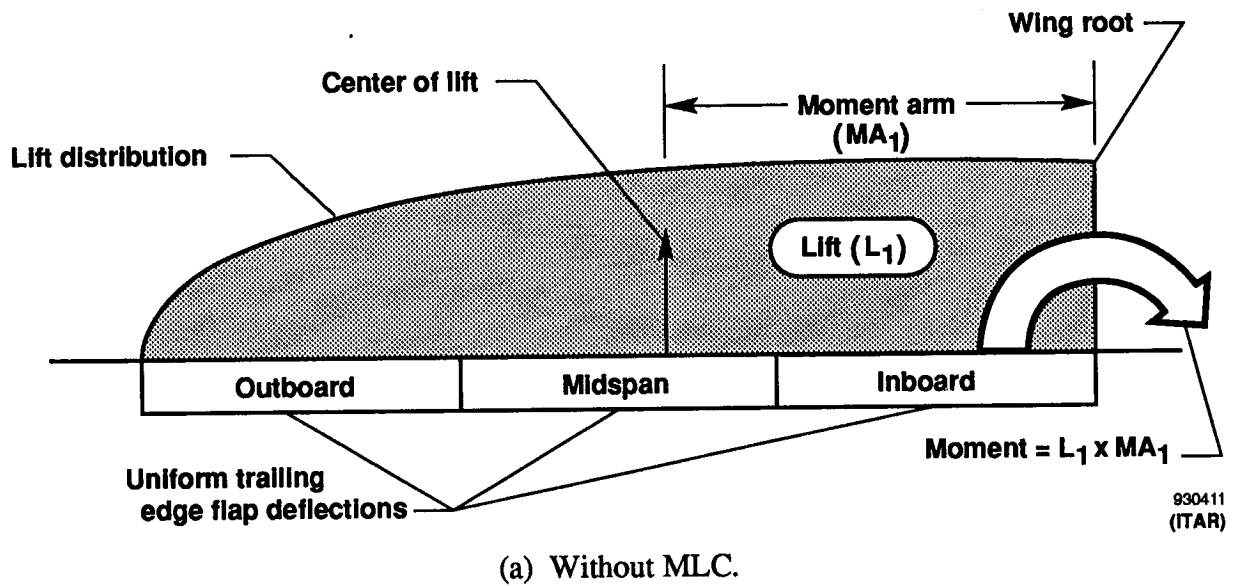
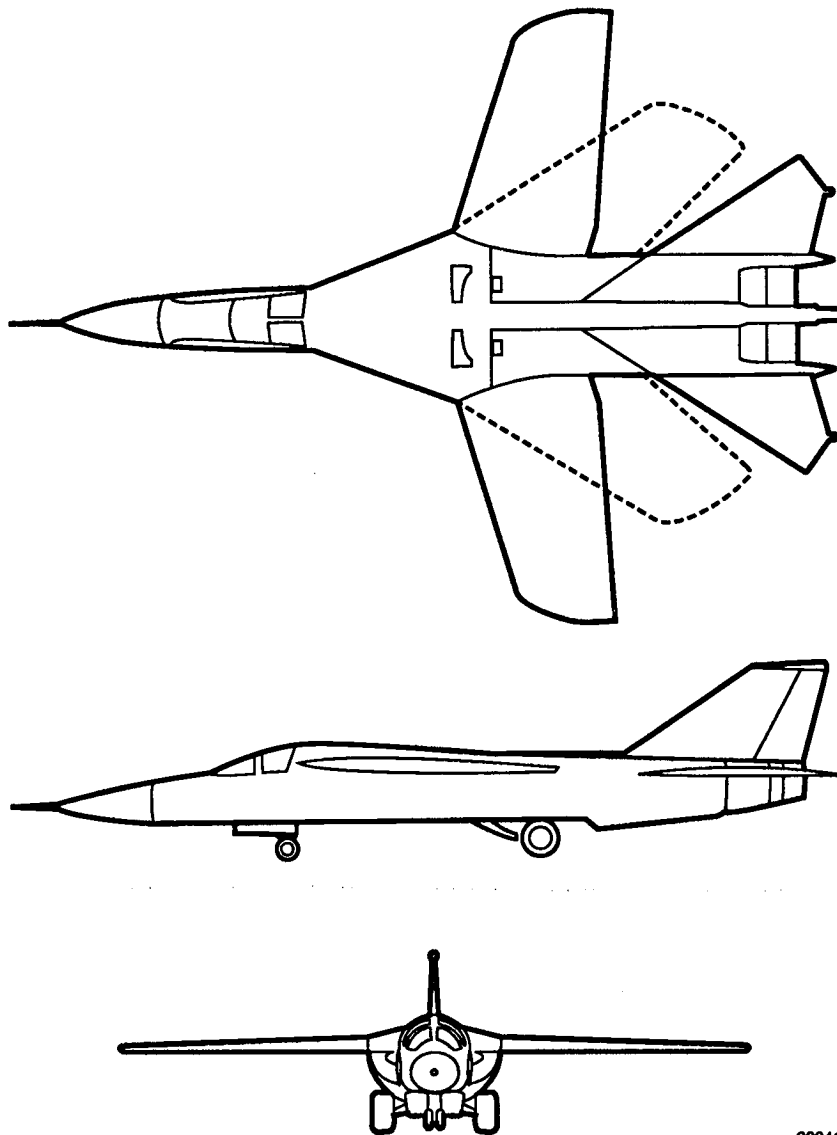


Figure 2. Spanwise lift distributions over wing semi-span and resulting reduced wing-root bending moment with MLC as compared with uniform maneuvering flap deflections where $L_1 = L_2$.

AIRCRAFT DESCRIPTION

The aircraft used in these experiments is an F-111A modified with a mission adaptive wing (MAW) having a supercritical airfoil with continuously variable smooth camber (ref. 2). Figure 3 shows three

views of the aircraft. Table 1 provides some of the detailed characteristics of the aircraft. As shown in figure 4, the leading-edge flaps comprise a single full-span segment on each wing. The trailing-edge flaps are divided into three segments per side. The inboard segments of the trailing edge function only as flaps. The midspan and outboard segments function both as ailerons and as flaps (flaperons). The wing camber can be controlled either manually or automatically by the onboard digital computers that monitor and control the wing configuration. The normal undeflected position of the flaps is 0/2/2, that is, $\delta_{LE} = 0^\circ / \delta_{TE} = 2^\circ / \delta_{TEO} = 2^\circ$, giving an airfoil shape that is a refinement of the supercritical airfoil used in the transonic aircraft technology (TACT) program (ref. 9). Illustrated also in figure 4 are the wing reference load axes. Wing-root bending is measured about vector **B**. Wing-root torsion is measured about vector **T**. Figure 5 illustrates the flexible fiberglass panels of the leading and trailing edges that provide the smooth variable-camber airfoil.

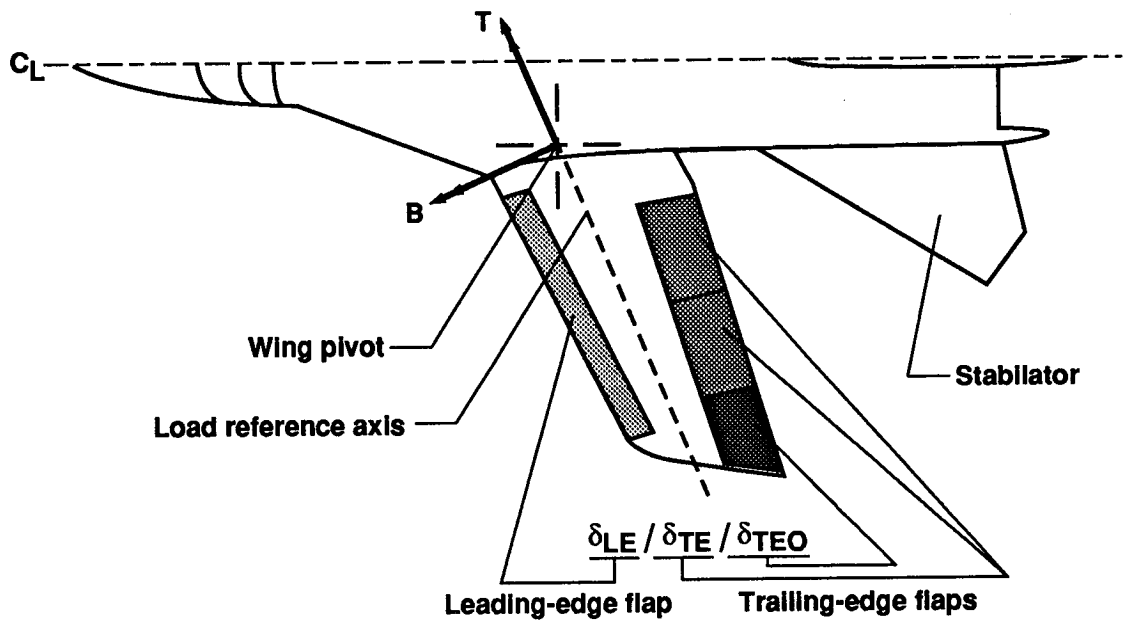


930413
(ITAR)

Figure 3. The AFTI/F-111 test aircraft.

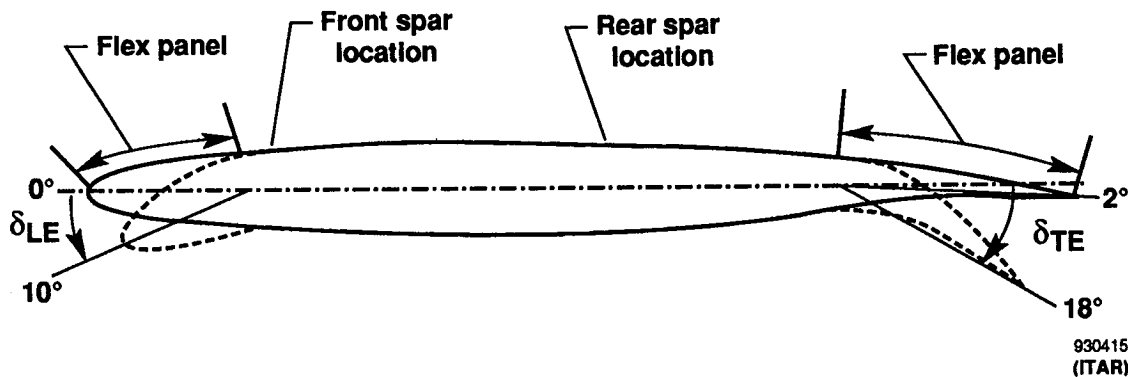
Table 1. AFTI/F-111 dimensions.

Wing (ref = 26° leading-edge sweep)		
Area		618.7 ft ²
Aspect ratio		4.95
Taper ratio (ref)		0.542
Span		664.1 in.
MAC		137.9 in.
Airfoil		Boeing Advanced Transonic (Boeing Company, Seattle, WA)
Sweep range		16–58°
Thickness ratio	root	9.7 percent
	tip	5.44 percent
Engine		
Two Pratt & Whitney TF30-P-9 turbofans (Pratt & Whitney, West Palm Beach, FL)		
Horizontal tail		
Total area (movable)		172.9 ft ²
Aspect ratio (movable)		2.12
Span		352 in.
Sweep, leading edge		57° 30'
Airfoil (root)		4 percent biconvex
Vertical tail		
Area		111.7 ft ²
Aspect ratio		1.419
Taper ratio		0.411
Sweep, leading edge		55°
Span		106.8 in.
Airfoil (root)		3.2 percent biconvex



930414
(ITAR)

Figure 4. Flap configuration nomenclature and loads axes.

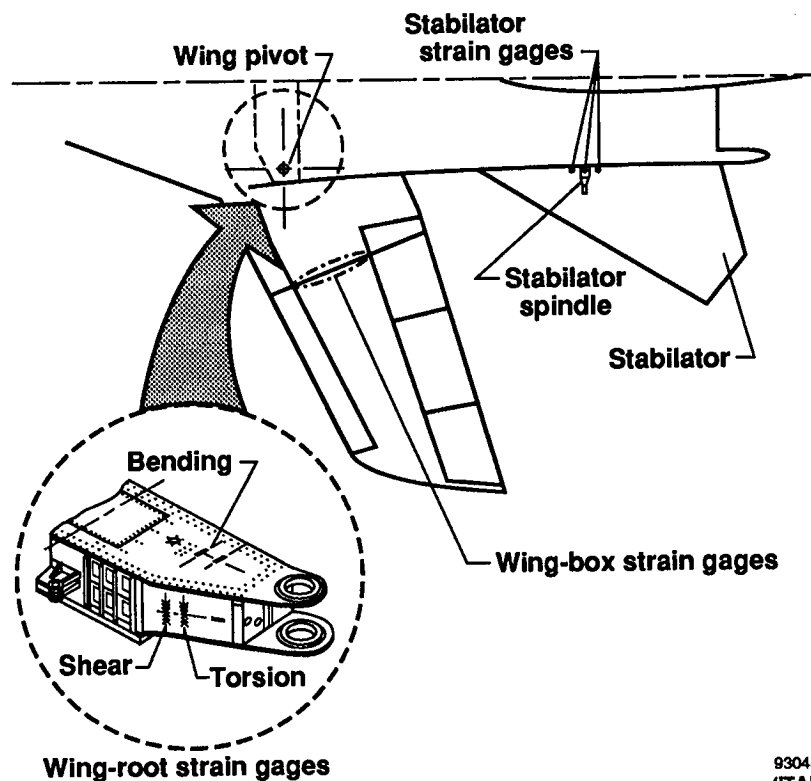


930415
(ITAR)

Figure 5. Smooth variable-camber airfoil on the AFTI-111.

INSTRUMENTATION

The aircraft was instrumented with strain gages on the left wing-box structure, at the left and right wing roots on the wing carry-through structure, and at the roots of the stabilators. Figure 6 shows these locations. The sensor devices used were bonded foil strain gages selected to match the thermal expansion properties of the structural members on which they were installed to minimize errors caused by apparent strain. The gages were used in the Wheatstone bridge circuit configuration and had four active arms. The loads parameters were recorded digitally at a rate of 20 samples/sec.

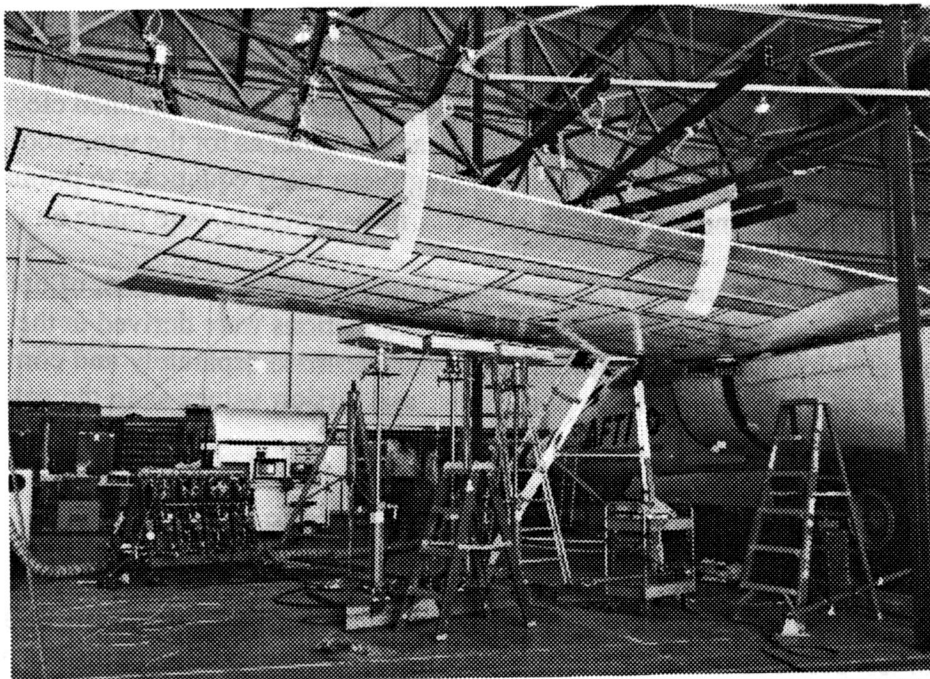


930485
(ITAR)

Figure 6. Instrumentation location.

The wing-root loads instrumentation was calibrated to measure structural loads at the center of the wing pivot by applying a series of single point loads to the lower surface of the wing using the methods described in reference 10. Figure 7 shows an example of the calibration setup including some of the load pad locations marked on the lower surface of the wing, the hydraulic loading jacks, the load cells, and the load pads used for a single load condition. The calibration strain-gage data were collected using digital data acquisition equipment. The data then were processed using an equation derivation program that calculates the influence coefficient of each bridge and derives the optimum equation for a specified set of gages. The best equations then were selected from the equations produced. All shear bridges on the left pivot support then were combined electrically into a single shear measurement signal for the left-wing root. All shear bridges on the right pivot support were combined into a single output for the right-wing shear measurement. Bending moment bridges and torsion bridges were electrically combined in a similar manner. Using trigonometric axis transformations, the resulting bending moment and torque values measured in the fuselage (or body) axes of the aircraft were converted to the wing load reference axes indicated in figure 4. With the wing leading edge swept to 26° , the reference axes were rotated approximately 24° from the body axes of the aircraft to coincide with axes of the primary wing spars. Table 2 provides additional information about each loads measurement.

During the loads calibration, several multiple-load-point tests also were performed. Multiple loads were applied at various distributed locations on the wing to simulate distributed airloads. The equations derived as described above then were validated using the data from the multiple-point check loads.



EC85-33050-012

Figure 7. Wing strain-gage calibration setup.

Table 2. Loads measurements definitions.

Forward spar web shear	Shear stress in the forward spar web at left wing station 81.5
Stabilator trim load	Stabilator shear at the root measured in the fuselage x - z plane
Wing-box bending moment	Bending moment about the chord line at left wing station 81.5
Wing-box shear	Wing shear resulting from lift measured at left wing station 81.5 in the wing x - z plane
Wing-box torsion	Torsion about the left wing 24.5 percent MAC line at left wing station 81.5
Wing-root bending moment	Bending moment about the x -axis measured at the center of the left wing pivot
Wing-root shear	Wing shear resulting from lift measured at the center of the left wing pivot in the x - z plane
Wing-root torsion	Torsion about the y -axis measured at the center of the left wing pivot

The wing-box strain gages were distributed along a left wingspan station located 81.5-in. outboard from the center of the left-wing pivot. This location was chosen as a convenient structural location that was far enough outboard from the pivot to monitor the loads in the individual spars. These gages were positioned on the various spars, the upper and lower wing skins, and the various spar webs. The outputs of the wing-box strain-gage bridges were recorded individually instead of being combined electrically as the wing-root gages were. Loads equations were derived in the same manner as for the wing-root gages. These individual signals were then combined mathematically using these loads equations to produce values for wing-box shear, bending moment, and torsion. No wing-box measurements were made on the right wing.

The stabilator strain gages were installed on and near the pivot spindle at the root of both the left and the right stabilator. These gages were calibrated and the loads equations were derived in the same manner as for the wing instrumentation. The gage output signals were recorded separately and combined mathematically to compute the resultant shear, bending moment, and torsion values as in the case of the wing box.

FLIGHT TEST CONDITIONS

Flight test data were obtained at Mach 0.6 to 0.9 and dynamic pressures ranged from 300 to 800 lb/ft², generating a matrix of test points as illustrated in figure 8. These combinations of conditions provided Reynolds numbers of 26×10^6 to 54×10^6 , based on the MAC. These flight conditions were chosen as representative of the range of conditions in the transonic and high subsonic flight conditions typical of fighter aircraft in highly loaded maneuvering flight. Because the 300 lb/ft² conditions could not produce limit loads, attention will be focused on the higher dynamic pressure conditions. The 10/18/18 baseline flap

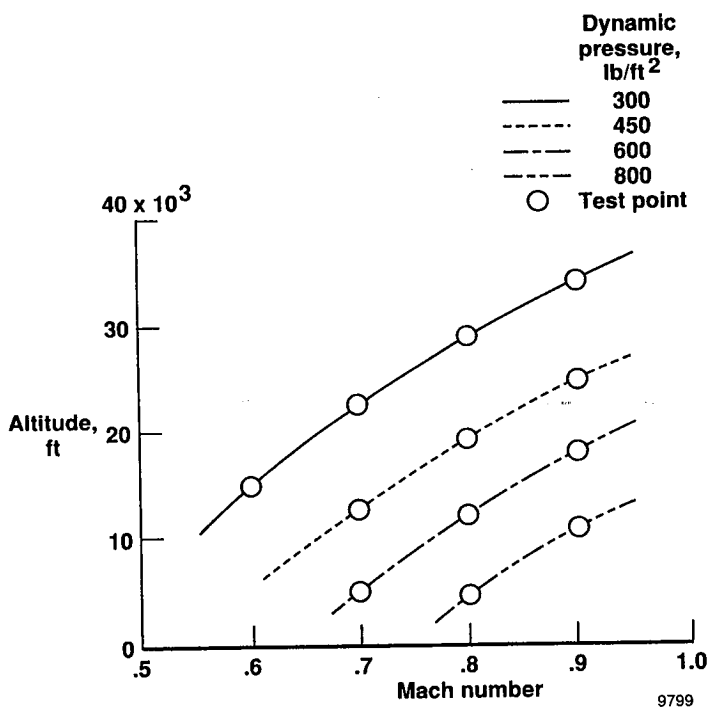


Figure 8. Flight loads test points.

configuration was flown only at 300 lb/ft² because of the very high drag produced. The 5/10/10 baseline flap configurations were flown at all test points. The flight test maneuvers used to gather these data were wind-up turns flown at constant Mach number and dynamic pressure in sets of three or more maneuvers, one at each of several specified flap settings. The maneuvers were flown in sets of three or more to minimize the change in fuel weight between flap configurations at a given set of flight conditions and thus facilitate comparisons among the measured loads. Maneuvers were rejected and repeated for which the Mach number deviated from the target value by more than ± 0.02 or for which dynamic pressure deviated by more than ± 10 percent of the target value. The gross weight for these maneuvers was constrained to the wing maneuver design point of 70,000 lb with a tolerance of $\pm 5,000$ lb. All maneuvers were flown at a leading-edge wing sweep of 26°.

As mentioned earlier, the nominal undeflected position of the flaps corresponds to a flap configuration of 0/2/2. The 5/10/10 flap setting was chosen as the baseline for configurations having moderate camber and as the basis of comparison for the partial and full MLC configurations. The 5/10/4 is an intermediate deflection, approximately halfway between the baseline and the full up position of the outboard flap segment. The 5/10/-1 setting is equivalent to the fully deployed MLC configuration, given the 5/10/10 manually set baseline. The 10/18/18 flap combination was chosen as the other baseline and corresponds to a high-camber configuration.

To evaluate the effect of a change in leading-edge deflection with the same baseline trailing-edge deflection, a flap setting of 10/10/10 was flown at 300 lb/ft² at three of the Mach numbers. These data enabled an estimate to be made of the relative contributions of the leading and trailing edges to the changes observed at the second baseline configuration, 10/18/18. Because the 5/10/10 and 10/18/18 settings were available among the discrete choices in the MAW control system, they were easily duplicated from one maneuver to another, thus substantially improving repeatability in the data. Flight conditions were selected to use the majority of the cleared subsonic envelope of the airplane.

Since this airplane also uses differential stabilator deflections (rolling tail) for roll control, the original plan was to fly the MLC maneuvers using fixed flaperons and rolling tail only for roll control to eliminate the effects of roll-control loads from the wing data. An evaluation of the two methods was made by flying one maneuver with flaperons fixed and one maneuver with flaperons active at the same conditions. Specified conditions of Mach and dynamic pressure were found to be more difficult to maintain in the maneuvers with the reduction in roll-control authority, particularly at the lower dynamic pressures. The additional time and flight cost of setting up the configuration to fly the test points with flaperons fixed did not justify the benefits (which proved to be slight) in the data collected. Therefore, all loads data presented were collected with the roll commands active on the flaperons.

RESULTS AND DISCUSSION

Although flight loads data were acquired at all of the Mach and dynamic pressure conditions indicated in figure 8, the loads data presented in this report in graphic form will consist of only those data needed to characterize and summarize the effects of maneuver load control on the airplane component loads. The planform geometry of an airplane has a strong influence upon the change in load distribution resulting from MLC. Figure 9 shows a planform diagram illustrating pitching moment forces for the AFTI/F-111 geometry. The change in incremental lift from the outboard flap deflection results in a change in pitching moment that, in turn, changes the horizontal tail trim loads. The force vectors in figure 9 illustrate the

beneficial effect occurring with MLC. The aft-swept wing places incremental outboard flap loads far aft of the c.g. Therefore, raising the outboard flap segment eliminates the incremental pitching moment generated by the outboard trailing-edge flap, thereby reducing the trim load requirement as compared with the baseline configuration. This trim load reduction is significant as will be seen in the discussion of the flight data.

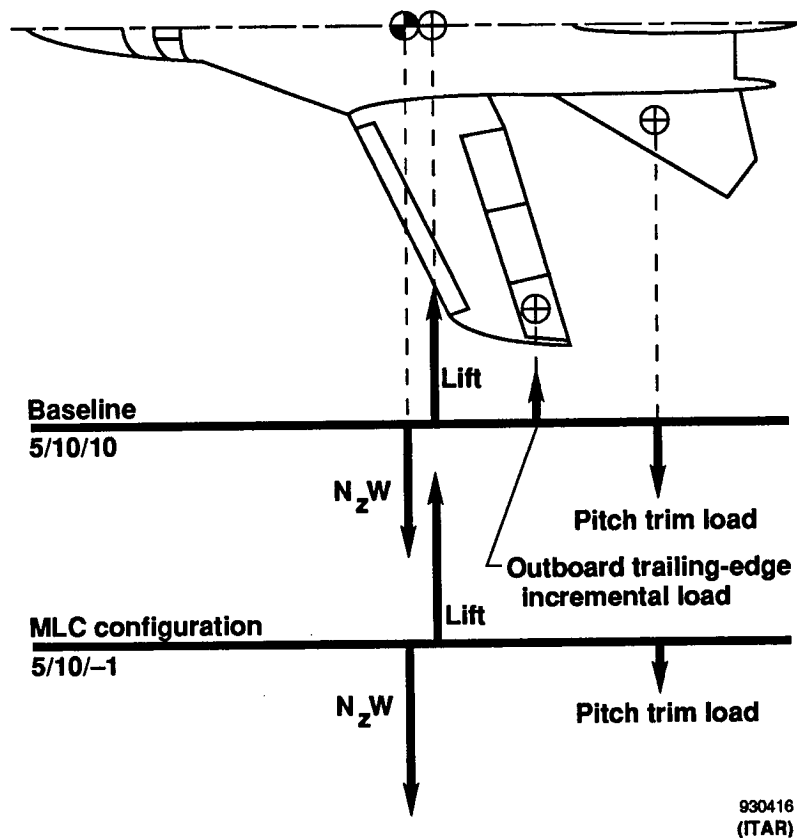
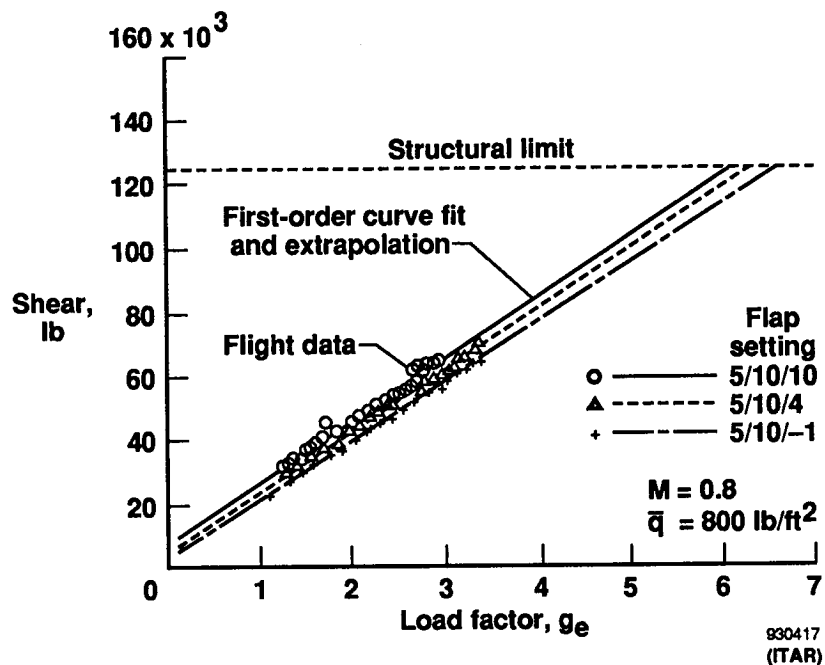


Figure 9. Forces and moments in the vertical plane at a given flight condition and center of gravity (aircraft shown in planform view for clarity).

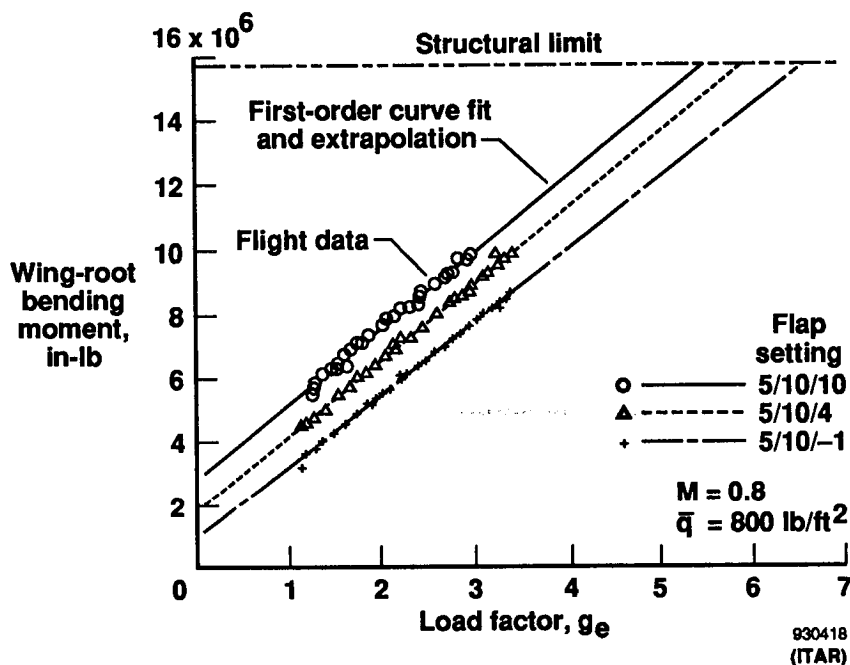
Wing-Root Loads

Figure 10 presents the wing-root shear, bending moment and torque loads as a function of equivalent load factor (g_e) at a dynamic pressure of 800 lb/ft² at transonic Mach numbers for a baseline camber of 5/10/10. By plotting the loads data as a function of equivalent load factor, the effects caused by small changes in aircraft weight from one maneuver to another are minimized and the flight loads presented are then representative of the aircraft loads at the design maneuver gross weight of 70,000 lb. The loads data are presented for three wing camber settings in which the leading-edge flaps were fixed at 5° and the in-board and mid-span trailing-edge flaps remained at 10°. The outboard trailing-edge flaps were positioned at 10° for the first maneuver, 4° for the second, and -1° for the third maneuver. First-order curves are fitted through the loads data and are extrapolated to the corresponding design limit load. Extending the extrapolated data through the structural limit value was done to show the difference in bending moment to be

expected at the structural limit with the MLC configuration. Other structural limits or severe buffet, however, may preclude reaching that point at some flight conditions. Other figures showing extrapolated data should be interpreted similarly.

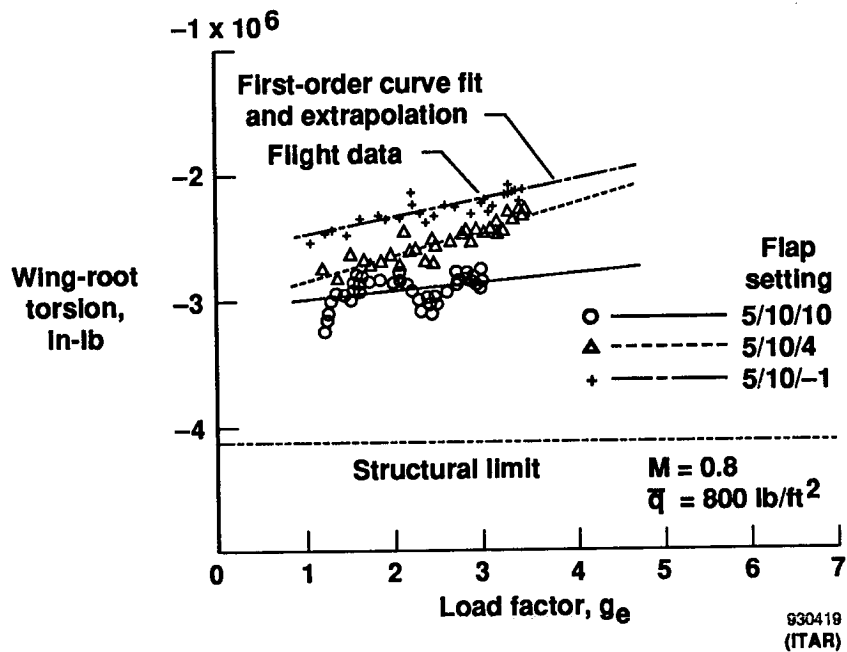


(a) Shear load.

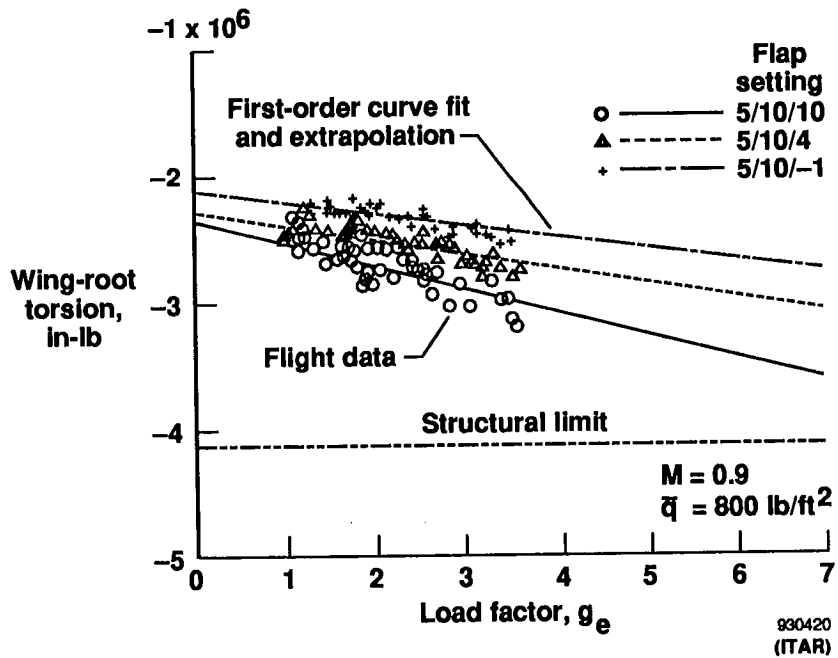


(b) Bending moment.

Figure 10. Wing-root data referenced to the wing axes for three flap configurations.



(c) Torsion (Mach 0.8).



(d) Torsion (Mach 0.9).

Figure 10. Concluded.

The data in figure 10(a) show that a small reduction in the wing-root shear load was achieved by raising the outboard trailing-edge flap. This small reduction in shear load is principally attributed to the corresponding reduction in the pitch trim load, which will be shown in a later figure.

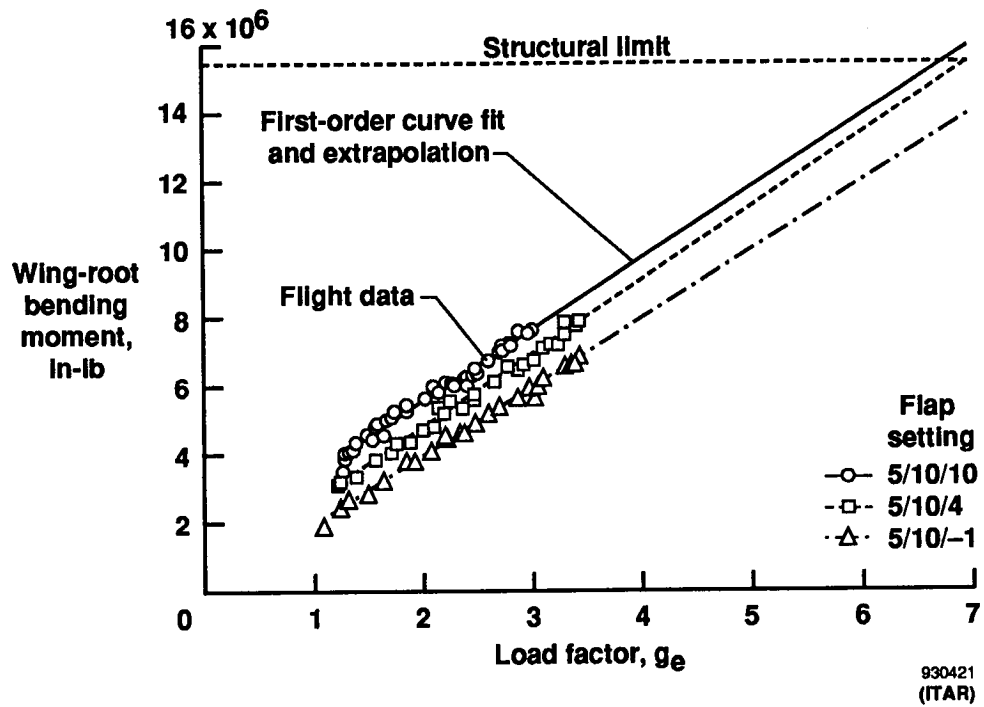
Perhaps the most important issue in an effort to reduce the wing loads through automatic scheduling of wing control surfaces is a desire to reduce the wing-root bending moment at a given load factor. For the AFTI/F-111, the wing-root bending moment represents the most critical loading parameter of the wing pivot structure. Figure 10(b) shows the effect of changing the position of the outboard trailing-edge flap segment on root bending moment. The extrapolated data out to the structural limit of 15.5×10^6 in-lb shows that an additional 1 g is available by raising the outboard trailing-edge flap segment up from 10° to -1° .

The shear and bending moment data shown for $M = 0.8$ in figures 10(a) and 10(b) are representative of the data at the other Mach numbers investigated. The wing-root torsion data (figs. 10(c) and 10(d)), however, display different trends with increasing load factor depending on Mach number. This difference results from the location of the load reference axis and the fact that the center of pressure on the wing moves aft with increasing Mach number at a given angle of attack (ref. 11). Figure 10(c) shows that at $M = 0.8$ the wing-root torsion decreases with both increasing load factor and the raising of the outboard trailing-edge flap. For this Mach number both variables have the effect of moving the torsional load away from the negative limit load toward zero load. The positive limit load is 2.54×10^6 in-lb (off the graph). At $M = 0.9$ (figure 10(d)), however, the center of pressure has moved aft of the load reference axis (fig. 3), which causes the torsional load to increase with increasing load factor. Thus, for the $M = 0.9$ condition, deflecting the outboard trailing-edge flap segment up alleviates the load which is approaching the structural limit as opposed to the Mach 0.8 case where the torsion load is moving away from the structural limit with increasing load factor.

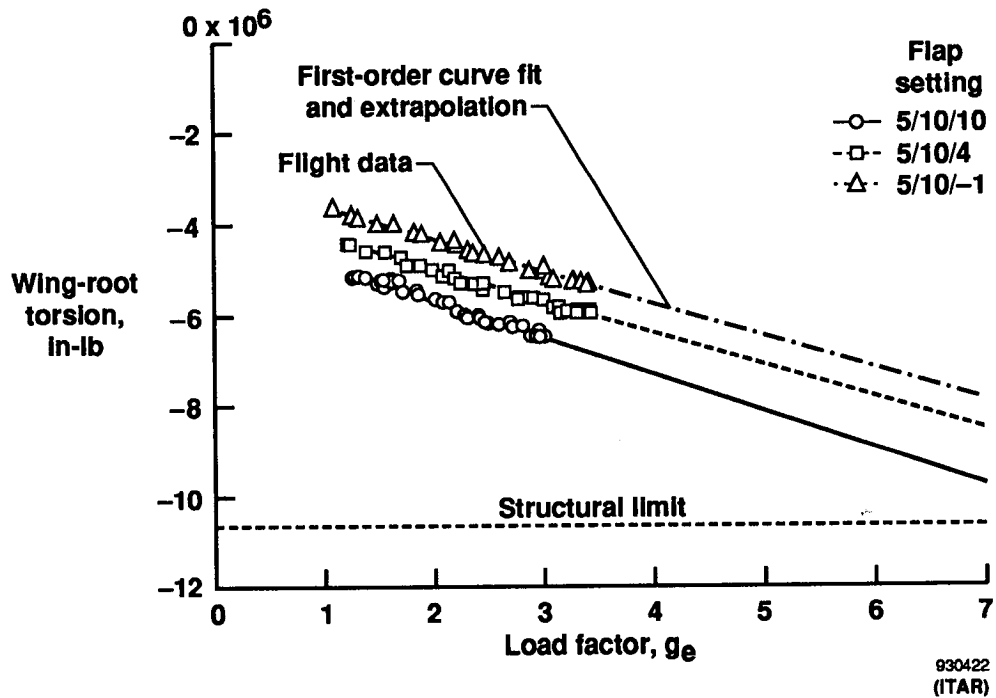
The data of figure 10 shows that the wing-root bending moment, which is the most critical load parameter for these conditions on the AFTI/F-111 aircraft, reaches its limit value at a lower load factor than that for either the shear or torsional loads. The shear load is the next most critical load parameter. Although the torsional load at the wing root has a large sensitivity to change in Mach number, a limit load value is never approached and is not a significant factor in implementing MLC in the AFTI/F-111 aircraft.

Figure 11 shows typical wing-root bending moments and torsion loads in the fuselage axes at the wing-root for the same set of maneuvers as compared in figure 10. The bending moments (fig. 11(a)) are necessarily somewhat less than those in the wing reference axes because of the geometry. The torsion loads (fig. 11(b)), however, are greater than those in the wing axes, again because of the geometry. The torsion loads also exhibit a different trend from those in figure 10(c) at the same conditions by showing a strong increase in value in response to increasing load factor. wing-root torsion is a critical structural design parameter for many of the flight maneuvering conditions where the wings are swept to larger sweep angles.

Figure 12 presents a summary of the loads benefits obtained in wing-root bending moment with the MLC flap configuration over the baseline (5/10/10) configuration. Over the dynamic pressure range of 450 to 800 lb/ft², the wing-root bending moment was reduced by 13 to 17 percent of the allowable limit value, tending to be slightly higher at the upper end of the Mach range. This change also can be interpreted as an incremental increase in limit load factor of 0.8 to 1.0 g above the nominal baseline limit of 4.5 g.

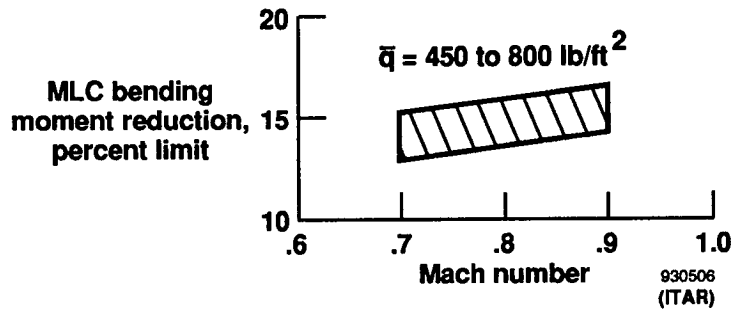


(a) Bending moment.

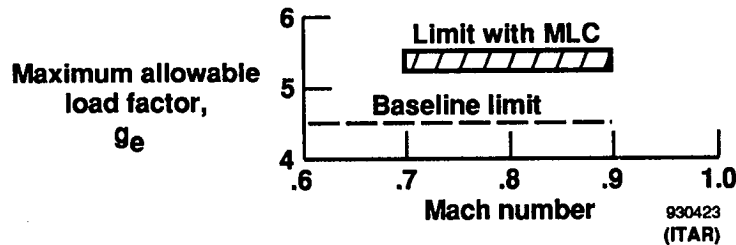


(b) Torsion.

Figure 11. Wing-root data referenced to the fuselage axes for three flap configurations, $M = 0.8$, $\bar{q} = 800 \text{ lb/ft}^2$.



(a) Range of bending moment reduction at constant equivalent load factor (g_e).



(b) Range of maximum allowable load factor with MLC compared with the baseline design limit load factor using uniform flap settings. Limits for this figure are determined by the maximum allowable wing-root bending moment.

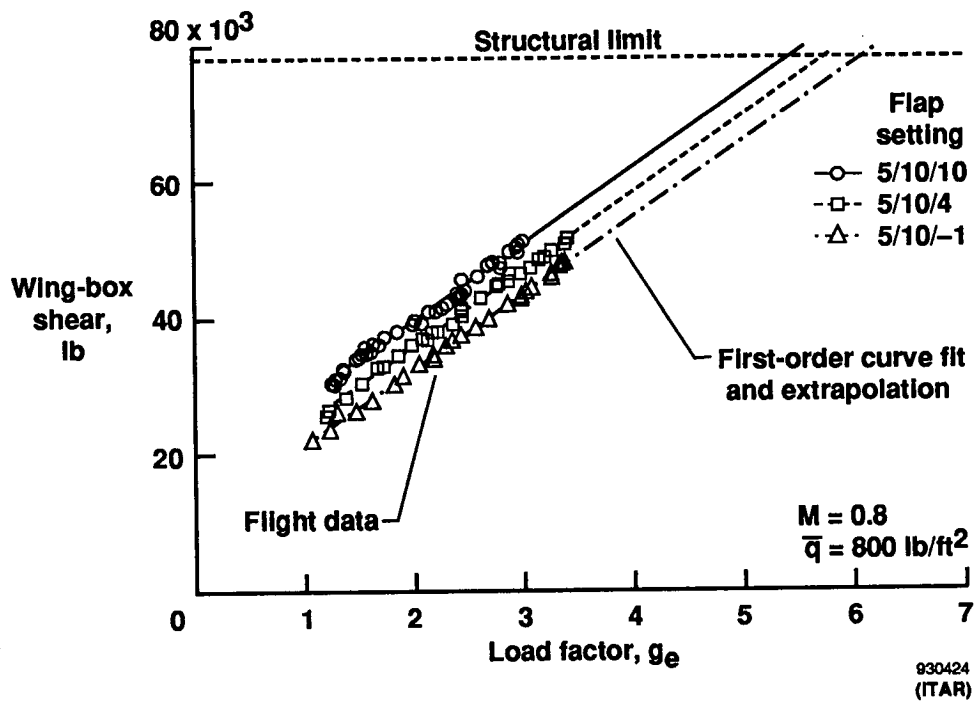
Figure 12. Structural and performance benefits produced with MLC for a range of flight test conditions for $M = 0.7$ to 0.9 .

Wing-Box Loads

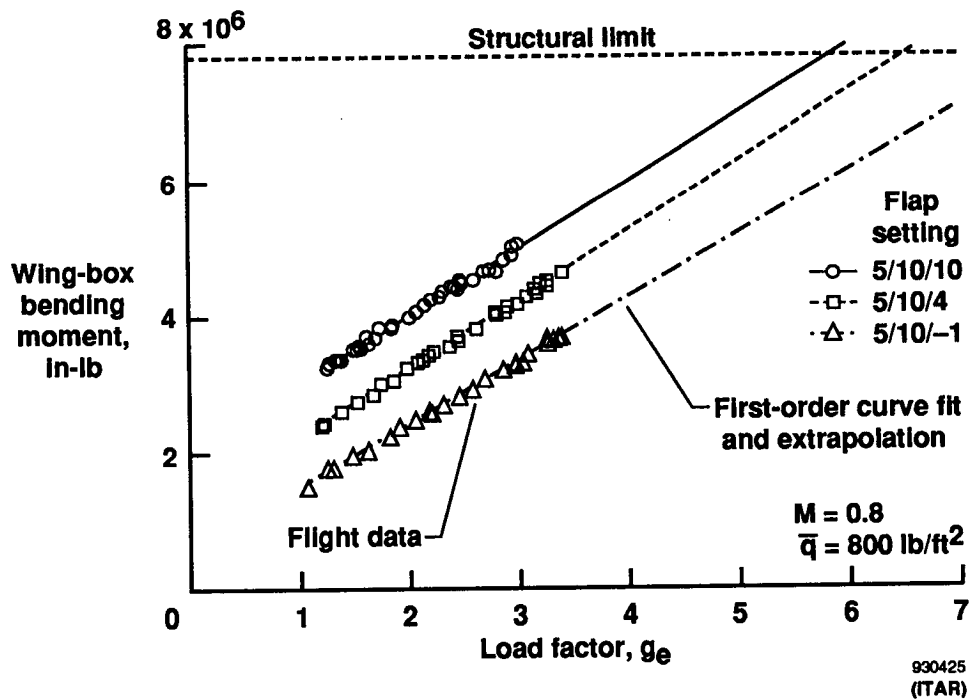
Attention is now turned to the loads in the wing box. Figure 13 shows wing-box shear, bending moment, and torsion loads data as measured about the wing axes for the 5/10/10 baseline and two MLC flap configurations as a function of equivalent load factor at a dynamic pressure of 800 lb/ft^2 . As for the wing-root data, the three outboard trailing-edge positions are 10° , 4° , and -1° . Again, first-order curves are fitted through the data and extrapolated to the corresponding design limit.

The data in figure 13(a) show that shear load reductions are achieved as the outboard trailing-edge flap segments are raised. Because the portion of the wing affected by the MLC configuration is proportionately larger than for the wing-root loads data, the load reduction is correspondingly larger. This effect can be seen by comparing figures 10(a) and 13(a).

Figure 13(b) shows the effects of MLC upon the wing-box bending moment. The load reduction potential at the design limit load factor is approximately 22 percent of the design limit load value. The percentage load reduction is greater at the wing-box instrumentation station than at the wing root, because a greater fraction of the wing outboard from that point is being reconfigured with MLC as stated above for shear. Therefore, the percentage of load reduction in the wing box is greater as seen by comparing figures 10(b) and 13(b).

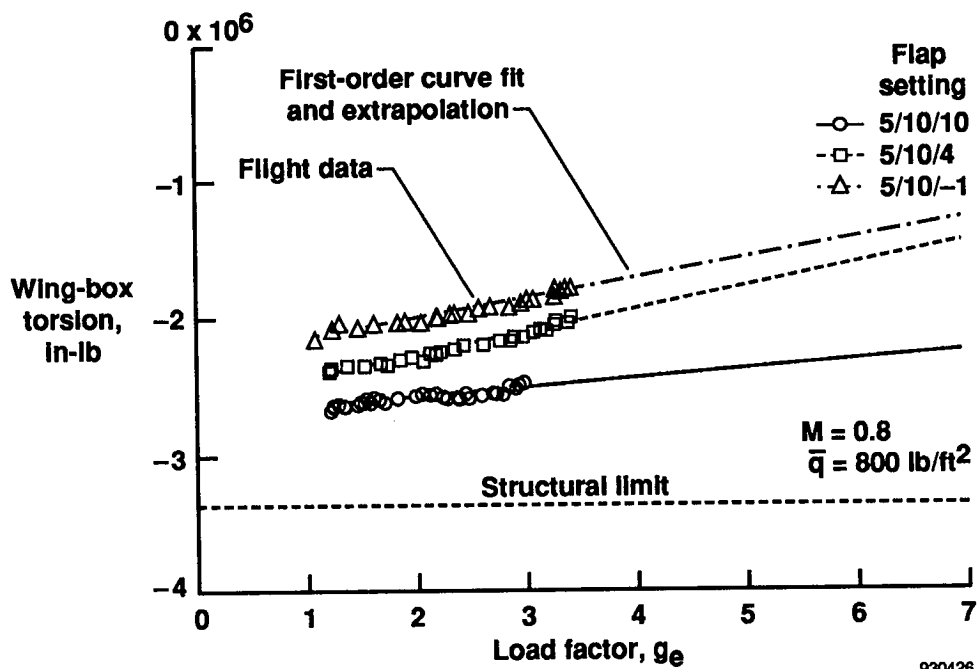


(a) Wing-box shear.

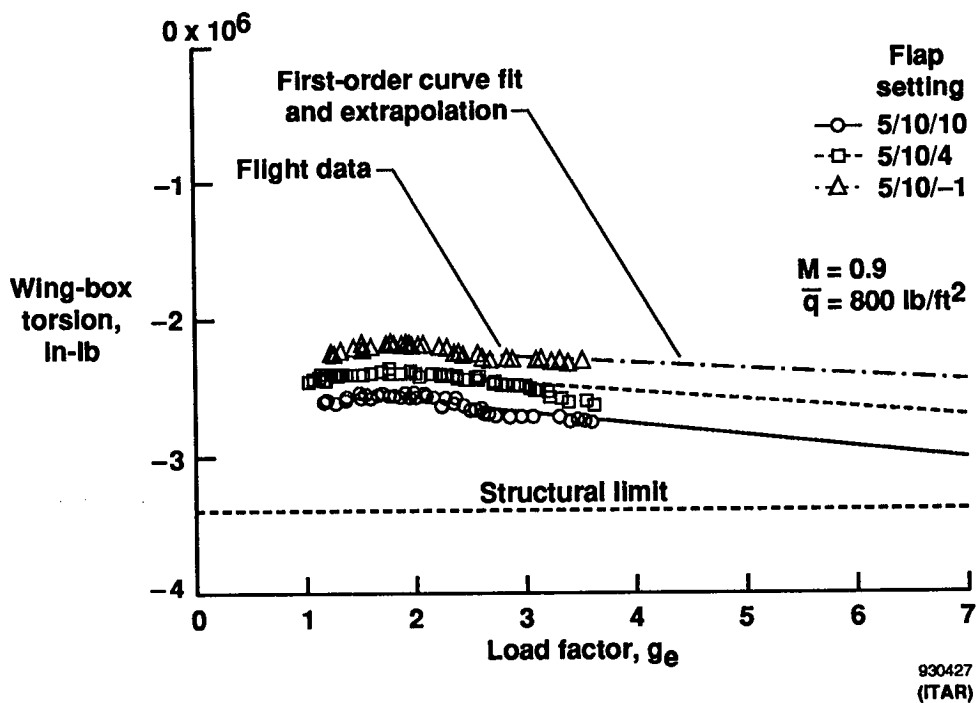


(b) Wing-box bending moment.

Figure 13. Wing-box data for three flap configurations.



(c) Wing-box torsion (Mach 0.8).



(d) Wing-box torsion (Mach 0.9).

Figure 13. Concluded.

Figure 13(c) shows the torsion load effect. As with the wing-root torsion, the wing-box torsion load is reduced with the MLC configuration. The wing-box torsion load also decreases with increasing load factor at or below 0.8 Mach number. However, as seen in figure 13(d), the torsion load increases with increasing load factor at 0.9 Mach number. This trend is the same as described for the wing root in the wing axes earlier. Wing-box torsion is a critical structural parameter for the AFTI/F-111, which can exceed its limit value in 1-g flight with trailing-edge flap deflection. Therefore, MLC load reduction could be used as a way to expand the flight envelope beyond what would otherwise be a firm structural limit in flight.

High-Camber Configurations

The previous discussion was based upon manual mode data from flight with a baseline flap configuration of 5/10/10. The following discussion will focus upon the manual mode 10/18/18 baseline flap configuration data, all of which were gathered in flight at a dynamic pressure of 300 lb/ft². To make the transition between the two configurations, it is useful to look at the effect of moving the leading edge from 5° of deflection to 10° while maintaining the flap settings at 10°. Figure 14 shows wing-root bending moment data from three maneuvers flown at Mach 0.8. The three flap configurations compared are 5/10/10, 10/10/10, and 10/18/18. Although the change in leading-edge position accounts for some of the increase in bending moment at a given load factor, the majority of the effect (approximately 75 percent) is a result of the change in trailing-edge position.

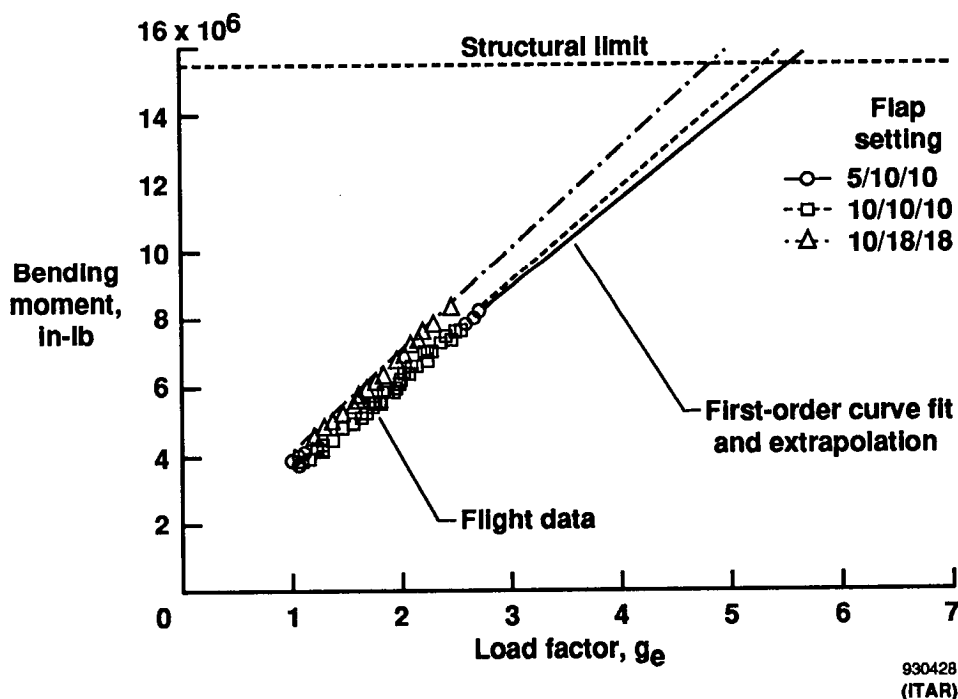


Figure 14. Effect of leading-edge flap deflection on wing-root bending moment referenced to the wing axes, $\bar{q} = 300 \text{ lb/ft}^2$, $M = 0.8$.

The 10/18/18 flap configuration represents a near-optimum configuration, as determined by wind-tunnel testing, for a high coefficient of lift of approximately 1.4 at low Mach numbers. The 18° deflection is the full flap deflection for the trailing-edge surfaces. The intermediate positions selected for the MLC investigation were 10/18/12 and 10/18/6. The fully configured MLC setting was 10/18/0. Figure 15 shows

wing-root bending moment data from four maneuvers, one for each stated flap configuration, at 0.8 Mach number. Again there is a substantial reduction in bending moment with the MLC configuration amounting to approximately 17 percent at limit load with 10/18/0 flaps. Wing-root shear, wing-root torsion, and the wing-box loads also exhibited load reductions similar to those found for the 5/10/10 baseline.

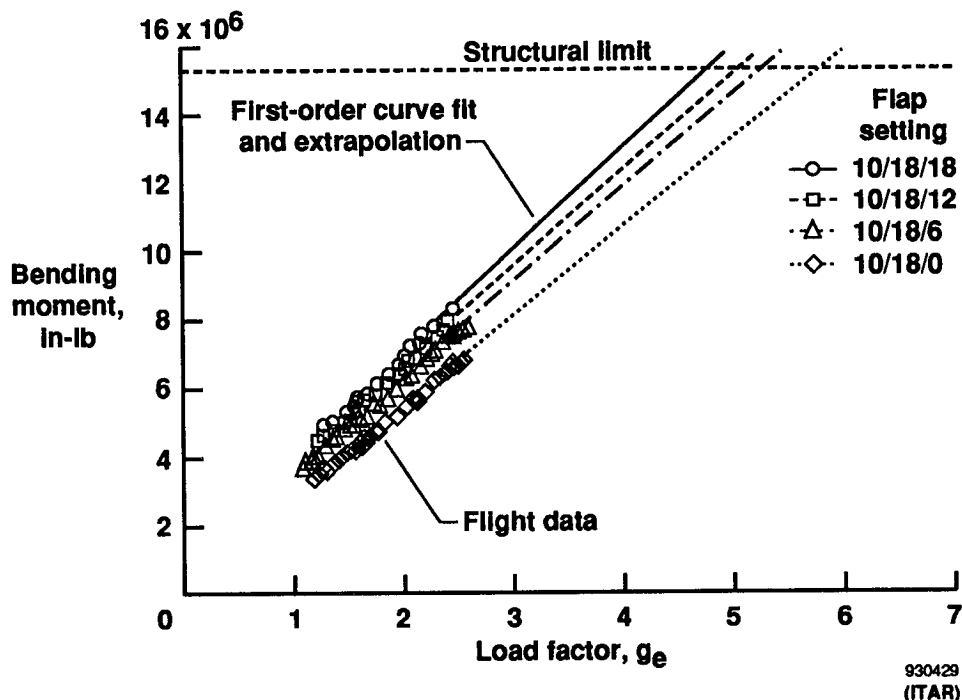


Figure 15. Wing-root bending moment referenced to the wing axes, $\bar{q} = 300 \text{ lb/ft}^2$, $M = 0.8$.

Forward Spar Web Shear

The shear stress in the forward spar web at the instrumented wing-box station also was monitored as an area of potential concern for the MLC testing. Figure 16 presents data from four maneuvers flown at $M = 0.8$ and a dynamic pressure of 600 lb/ft^2 . As a basis of comparison, the first maneuver was flown with the flaps in the 0/2/2 or flaps up configuration. The other three were a set of MLC maneuvers using the 5/10/10 baseline. From the figure, for the range of conditions flown, a small reduction, rather than an increase, is seen in the forward spar shear stress with the additional camber.

Stabilator Pitch Trim Loads

Figure 17 presents stabilator loads and stabilator position data. The effect on stabilator pitch trim loads of changing the position of the outboard trailing-edge flap segment is shown in figure 17(a) for a dynamic pressure of 800 lb/ft^2 . Figure 17(b) presents the corresponding stabilator deflections for these two maneuvers. For trimmed flight, the algebraic sum of the left- and right-stabilator shear loads is the trim load in pitch upon the aircraft. Although the data appear to be quite noisy, they include both roll and pitch control input loads which causes the irregular load levels. First-order curves are fitted through the data for ease of comparison. The magnitude of the pitch trim force increased with increasing dynamic pressure, as one would expect. The reduction in trim load is attributed as the cause of the reduction of wing shear load as noted earlier and as a part of the cause for a beneficial effect that MLC has on aircraft performance, which

will be discussed later. For all conditions tested the trim loads remained small compared with the structural limit for stabilator shear (left and right combined) of 138,000 lb for this aircraft.

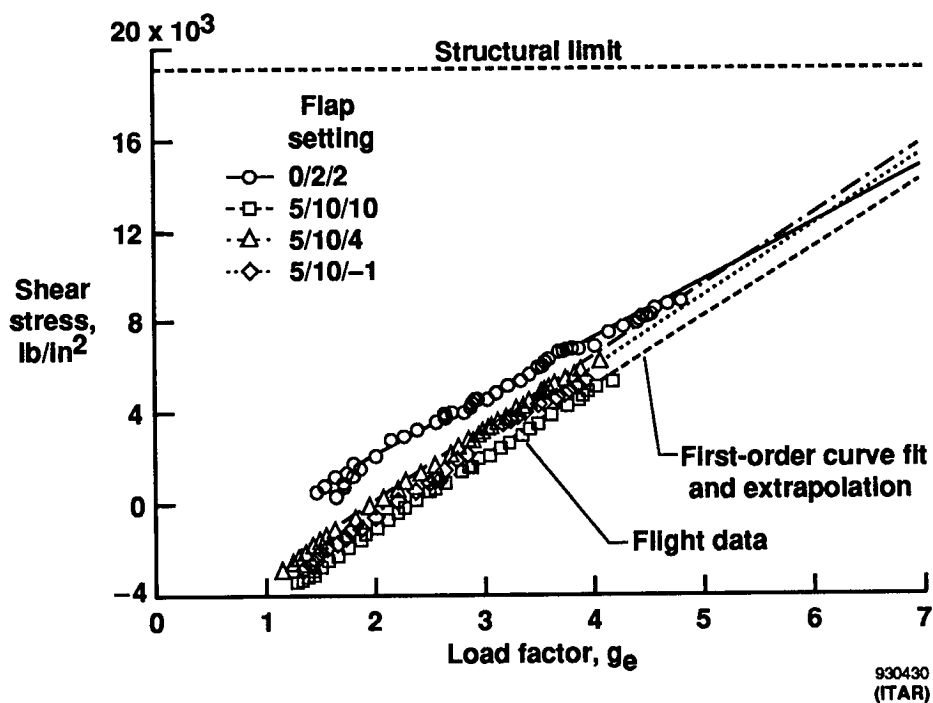
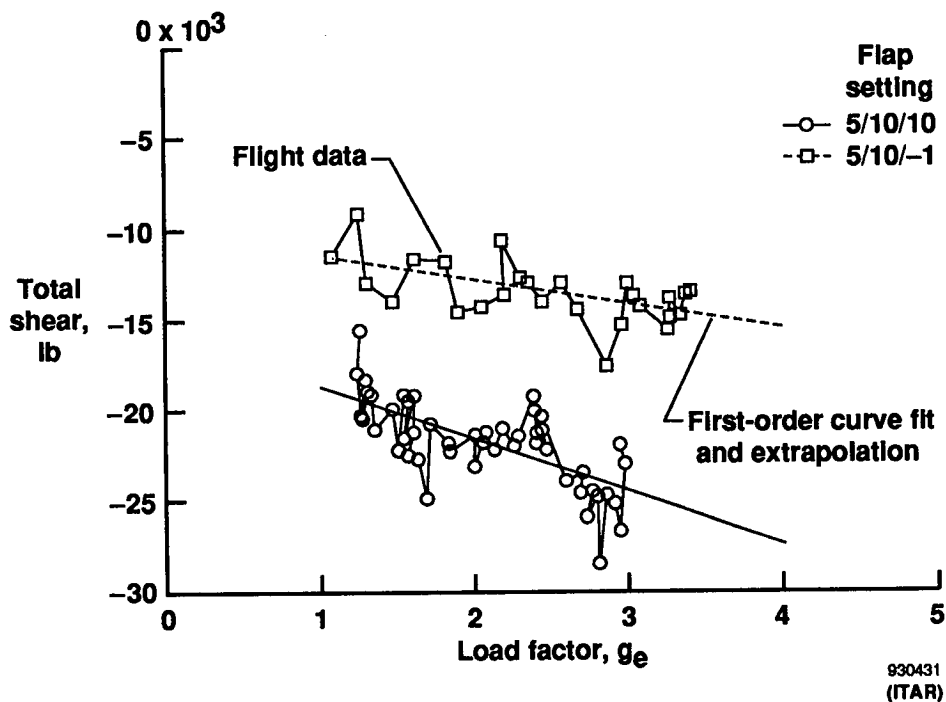
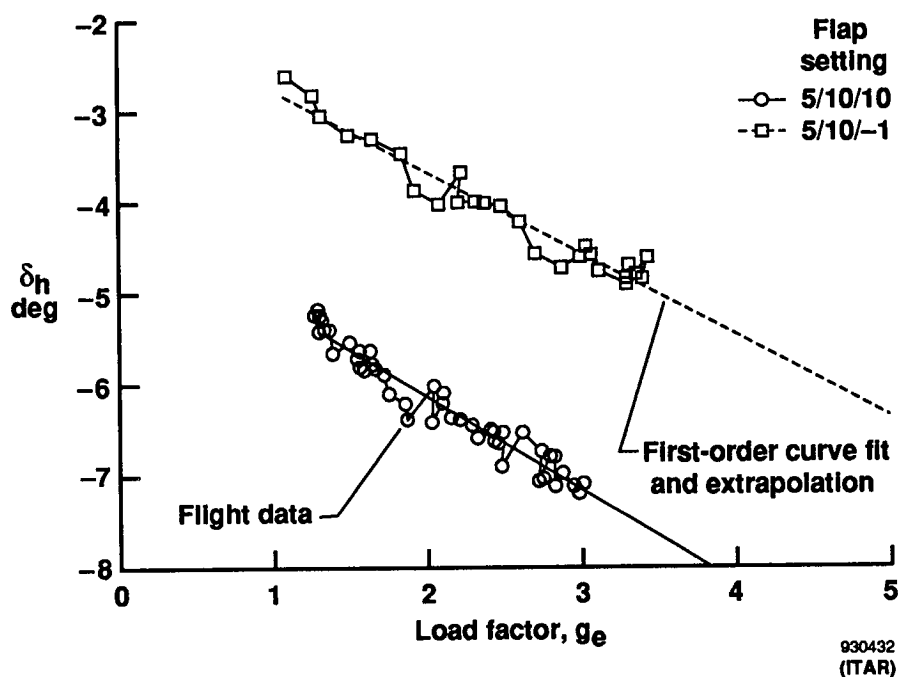


Figure 16. Forward spar web shear stress, $M = 0.8$, $\bar{q} = 600 \text{ lb/ft}^2$.



(a) Stabilator trim loads.

Figure 17. Stabilator trim loads and corresponding stabilator pitch trim deflections at $M = 0.8$, $\bar{q} = 800 \text{ lb/ft}^2$.



(b) Stabilator deflection.

Figure 17. Concluded.

Automatic Modes

The previous discussion has focused on the load effects of simulating MLC using manually configured flaps with variations about the 5/10/10 and 10/18/18 baselines. Now the focus will turn to the effects observed when MLC was used in its automatic mode, which computes a wing-root bending moment as a function of flap position, airspeed, Mach number, dynamic pressure, normal acceleration, and wing sweep position and automatically raises the outboard flaps when a preset threshold is exceeded. MLC was designed to be used with the MCC mode which uses current values of dynamic pressure, Mach number, gross weight, and normal acceleration to maximize the aircraft L/D by continuously and automatically repositioning both leading and trailing-edge flaps according to the predefined lookup table. With both the MCC and MLC automatic modes engaged, the flaps to move downward as the load factor increases from a flap configuration near 0/2/2 (the nominal flaps-up position) for typical cruise conditions to a progressively higher camber setting per the flap schedule as load factor increases. If the computed bending moment reaches the preset threshold value, MLC then overrides the MCC commands to the outboard trailing-edge segments and commands them to move rapidly to their extreme full up position (-1°) until the load factor decreases and the computed bending moment again falls below the threshold. For testing purposes the threshold was usually set well below the allowable limit. In actual production use, however, the threshold would probably be set at approximately 95 percent of the allowable limit for bending moment.

Four load maneuvers were flown with Mach numbers ranging from 0.7 to 0.9 with a dynamic pressure of 450 lb/ft^2 using MCC together with the MLC mode active. Figure 18 compares a typical maneuver with fixed flaps with a typical MCC/MLC maneuver at similar flight conditions. The fixed flap maneuver, having a constant and initially greater flap deflection, produced higher bending moments throughout the

load factor range encountered. The maximum α reached on this maneuver was 9.9° . Between 1 and 3 g , the MCC/MLC maneuver shows a steeper slope as MCC increased the flap deflection to a value of approximately 3/6/6 in response to the rising load factor, at which point the computed bending moment reached the preselected MLC threshold. The bending moment then remained essentially constant until MLC drove the outboard flaps to the full up position of approximately 5/8/-1. Then the bending moment continued to rise as load factor and MCC flap deflection continued to increase. The maximum α reached was 15.8° . This figure is typical of results produced with the MCC/MLC combination. By comparing the two maneuvers of figure 18 it is seen that approximately 1.0 g more load factor is available for a given wing-root bending moment (e.g., 10×10^6 in-lb) with MLC.

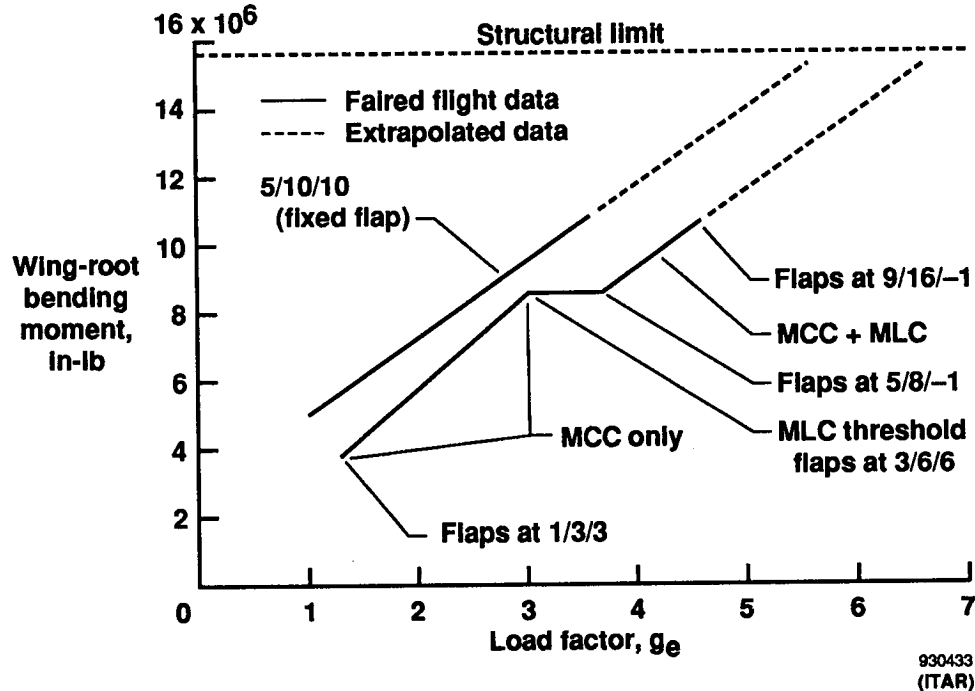
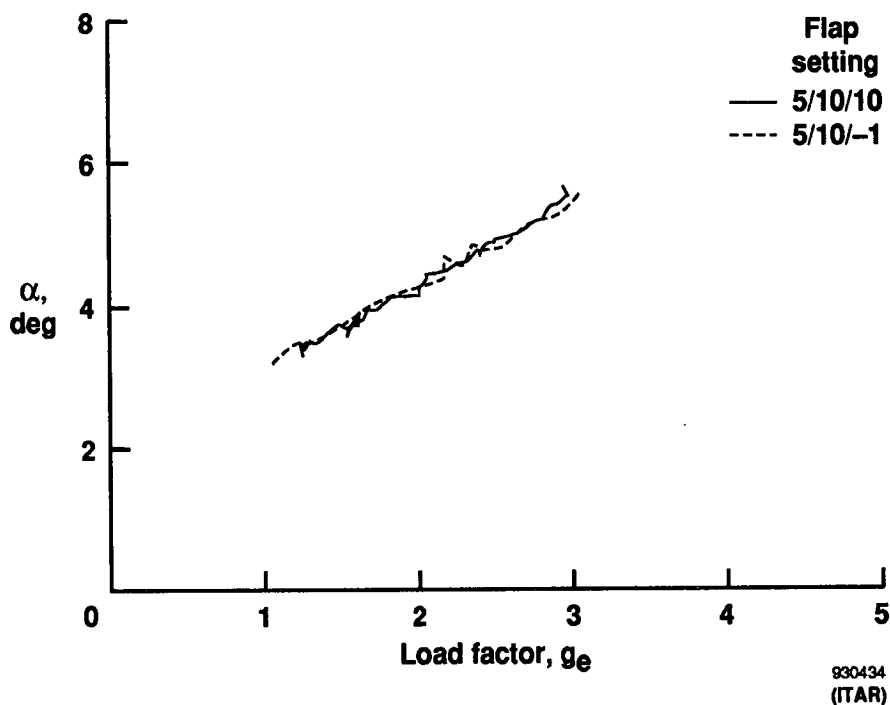


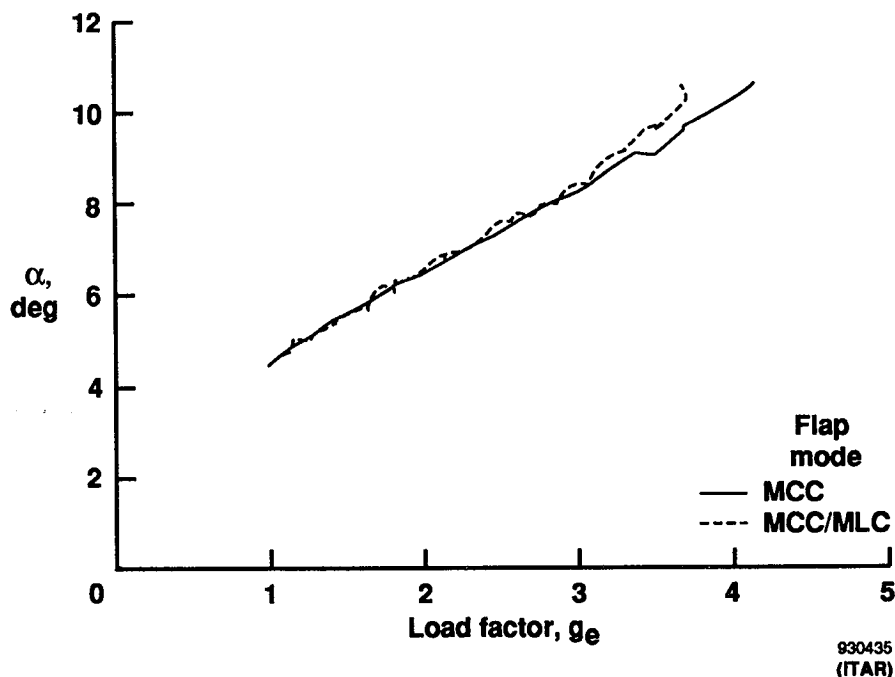
Figure 18. Wing-root bending moment for fixed flap configuration and for MCC/MLC at $M = 0.7$, $\bar{q} = 450 \text{ lb/ft}^2$.

Typical data presented in figure 19 are shown to compare the changes in angle of attack for a pair of manual mode maneuvers and a pair of automatic mode maneuvers. Figure 19(a) shows the angle of attack for 5/10/10 and 5/10/-1 maneuvers. While it could be assumed that a substantial increase in angle of attack would be necessary to maintain the same load factor with the MLC flap configuration because of the loss of camber on the outboard portion of the wing, any difference in the angle of attack for these maneuvers is not readily distinguishable. The lack of an appreciable change in angle of attack is attributed to the reduction in the trim load required. Figure 19(b) shows data from two automatic mode maneuvers, one with MCC only and the other with both MCC and MLC engaged. In this comparison, the two curves again are essentially indistinguishable up to an angle of attack of approximately 8° , then begin to diverge with the MCC/MLC configuration requiring the higher value for a given load factor. This difference, where the angle of attack is greater than 8° , is attributed to the onset of separated flow, which is aggravated by the discontinuity at the gap between the mid and outboard flap segments. Note that the MLC flap position schedule was derived from wind-tunnel data and was not revised using flight data to refine the

optimization. Therefore, it is possible with further optimization of the flap schedule that the loads benefits expected would change, although any such change is likely to be relatively small.



(a) Manual mode, $M = 0.8$, $\bar{q} = 800 \text{ lb/ft}^2$.



(b) Automatic modes, $M = 0.8$, $\bar{q} = 450 \text{ lb/ft}^2$.

Figure 19. Angle-of-attack comparisons for manual mode and automatic modes.

The effect of the MLC flap configuration upon aircraft performance became a topic of interest when the large reduction in pitch trim load was observed. Reference 12 provides much more detail regarding the effects of the automatic modes upon performance. Figure 20, which was derived from figure A31 of reference 12, compares drag polars from two maneuvers flown with (a) MCC active and (b) both MCC and MLC active. Note the small C_L improvement that occurs during the first few degrees of MLC outboard flap travel. Then the curves converge and cross, indicating a small performance penalty with the outboard segment in the full up position. The MCC/MLC line segment labeled "MLC transition" indicates the portion of the maneuver during which the outboard flap segments were moving from the nominal MCC position to the full up position. The reduction in trim load and, therefore, reduction in trim drag appear significant in the small improvement in aircraft performance where the angle of attack is less than 10° . This point is where the angle of attack increase is noted in the previous figure. Other possible contributors to the drag improvement are discussed in reference 12. Among these is a potential drag reduction that has been reported with the use of differentially set roll control surfaces.

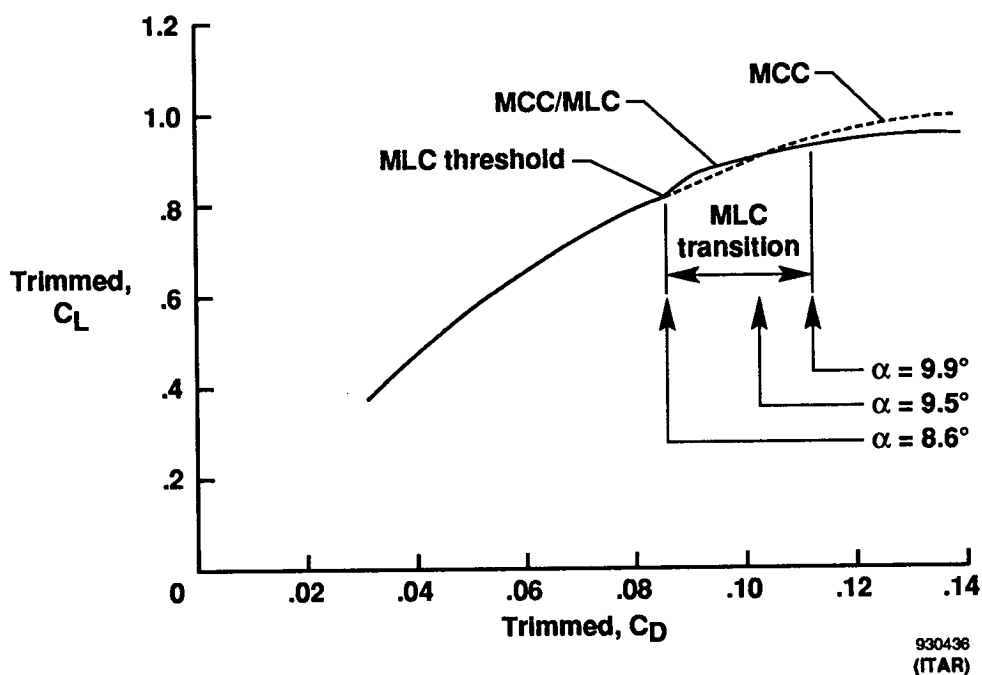


Figure 20. MLC effect on performance at $M = 0.8$, $\bar{q} = 300 \text{ lb/ft}^2$.

Buffet onset for this aircraft occurs at an angle of attack of approximately 10° (ref. 13). Therefore, maneuvering in the region above 10° angle of attack would be minimized because of heavy buffet, especially at high dynamic pressures. Note also that, as mentioned earlier, the normally envisioned use of MLC is to set the threshold at a value very close to the maximum bending moment allowable rather than at a value somewhat less than the allowable as was the case in most of the test maneuvers flown. Therefore, maneuvering at a substantially higher load factor than that which produces bending moments much in excess of the MLC threshold would probably not be done in actual practice for this aircraft. That is, it is unlikely that the performance loss that is apparent at angles of attack above 10° is significant, because the aircraft would also probably be in heavy buffet at high dynamic pressures.

CONCLUDING REMARKS

A comparison of aircraft component loads data between a maneuver load control (MLC) flap configuration and a baseline configuration using manually positioned, uniformly deflected flaps has been presented for an aircraft having a modified supercritical wing with a continuously variable camber airfoil. Flight test data were collected at Mach 0.6, 0.7, 0.8, and 0.9 and dynamic pressures tested were 300, 450, 600, and 800 lb/ft². All data presented were obtained at a wing-sweep position of 26° and compared with a baseline flap configuration.

Significant load reductions were obtained at all flight conditions tested with the MLC configuration. For dynamic pressures of 450 to 800 lb/ft², increases in load factor of 0.8 to 1.0 g were achieved with the MLC flap configuration at the same wing-root bending moments measured for the corresponding baseline flap configuration. Although wing-root torsion load reductions resulting from MLC were found throughout the Mach-number range flown, the most beneficial effect for torsion was seen at Mach 0.9.

Horizontal tail pitch trim loads also were reduced significantly with the MLC flap configuration. This trim load reduction may be responsible for the small beneficial effect which MLC had on aircraft performance for some flight conditions where the angle of attack was less than 10°.

*Dryden Flight Research Facility
National Aeronautics and Space Administration
Edwards, California, August 8, 1993*

REFERENCES

1. Mechtly, E.A., *The International System of Units - Physical Constants and Conversion Factors, Second Revision*, NASA SP-7012, 1973.
2. Powers, Sheryll Goecke, ed., *Advanced Fighter Technology Integration F-111 Mission Adaptive Wing*, symposium proceedings published as NASA CP-3055, (ITAR), 1990.
3. Thornton, Stephen V., *Structural Loads With Maneuver Load Control for the Advanced Fighter Technology Integration/F-111 Mission Adaptive Wing*, NASA TM-4404, 1992.
4. Hall, Joseph M., *AFTI/F-111 Flight Control System*, AFWAL-TR-87-3012, Flight Dynamics Laboratory, Air Force Wright Aeronautical Laboratories, Air Force Systems Command, Wright-Patterson Air Force Base, Ohio, Dec. 1987.
5. Anderson, D.C., R.L. Berger, and J.R. Hess, Jr., "Maneuver Load Control and Relaxed Static Stability Applied to a Contemporary Fighter Aircraft," AIAA 72-870, AIAA Guidance and Control Conference, Stanford, California, Aug. 1972.
6. White, Roland J., "Improving the Airplane Efficiency by Use of Wing Maneuver Load Alleviation," AIAA 70-877, CASI/AIAA Meeting on the Prospects for Improvements in Efficiency of Flight, Toronto, Canada, July 1970.
7. Hodges, Garold E., and James R. McKinzie, "B-52 Control Configured Vehicles Maneuver Load Control System Analysis and Flight Test Results," AIAA 75-72, AIAA 13th Aerospace Sciences Meeting, Pasadena, California, Jan. 1975.
8. North American Rockwell Corporation, *Analysis of Relaxed Static Stability and Maneuver Load Control Applications to a Large Bomber*, AD-784865, Dec. 1971.
9. Baldwin, Wayne, ed., *Symposium on Transonic Aircraft Technology (TACT)*, AFFDL 78-100, Air Force Flight Dynamics Laboratory, Wright-Patterson Air Force Base, Ohio, Aug. 1978.
10. Skopinski, T.H., William S. Aiken, Jr., and Wilber B. Huston, *Calibration of Strain-Gage Installations in Aircraft Structures for the Measurement of Flight Loads*, NACA Rept. 1178, 1954.
11. Webb, Lannie D., Sheryll Goecke Powers, and Lucinda A. Rose, *Selected Local Flow-Field Measurements on the Advanced Fighter Technology Integration (AFTI)/F-111 Aircraft Mission Adaptive Wing*, NASA TM-4405, 1992.
12. Phillips, W. Paul, "Lift and Drag Characteristics of the AFTI/F-111 With the MAW Automatic Control Modes," *Advanced Fighter Technology Integration F-111 Mission Adaptive Wing*, NASA CP-3055, 1990, pp. 263-283.
13. Friend, Edward L., and Jeffrey M. Thompson, "Buffet Characteristics of the Advanced Fighter Technology Integration (AFTI)/F-111 Airplane with the Mission Adaptive Wing," *Advanced Fighter Technology Integration F-111 Mission Adaptive Wing*, NASA CP-3055, 1990, pp. 197-222.

REPORT DOCUMENTATION PAGE			Form Approved OMB No. 0704-0188	
<small>Public reporting burden for this collection of information is estimated to average 1 hour per response, including the time for reviewing instructions, searching existing data sources, gathering and maintaining the data needed, and completing and reviewing the collection of information. Send comments regarding this burden estimate or any other aspect of this collection of information, including suggestions for reducing this burden, to Washington Headquarters Services, Directorate for Information Operations and Reports, 1215 Jefferson Davis Highway, Suite 1204, Arlington, VA 22202-4302, and to the Office of Management and Budget, Paperwork Reduction Project (0704-0188), Washington, DC 20503.</small>				
1. AGENCY USE ONLY (Leave blank)		2. REPORT DATE September 1993		3. REPORT TYPE AND DATES COVERED Technical Memorandum
4. TITLE AND SUBTITLE Reduction of Structural Loads Using Maneuver Load Control on the Advanced Fighter Technology Integration (AFTI)/F-111 Mission Adaptive Wing				5. FUNDING NUMBERS WU 505-63-50
6. AUTHOR(S) Stephen V. Thornton				
7. PERFORMING ORGANIZATION NAME(S) AND ADDRESS(ES) NASA Dryden Flight Research Facility P.O. Box 273 Edwards, California 93523-0273				8. PERFORMING ORGANIZATION REPORT NUMBER H-1940
9. SPONSORING/MONITORING AGENCY NAME(S) AND ADDRESS(ES) National Aeronautics and Space Administration Washington, DC 20546-0001				10. SPONSORING/MONITORING AGENCY REPORT NUMBER NASA TM-4526
11. SUPPLEMENTARY NOTES				
12a. DISTRIBUTION/AVAILABILITY STATEMENT Unclassified--Unlimited Subject Category 02				12b. DISTRIBUTION CODE
13. ABSTRACT (Maximum 200 words) A transonic fighter-bomber aircraft, having a swept supercritical wing with smooth variable-camber flaps was fitted with a maneuver load control (MLC) system that implements a technique to reduce the inboard bending moments in the wing by shifting the spanwise load distribution inboard as load factor increases. The technique modifies the spanwise camber distribution by automatically commanding flap position as a function of flap position, true airspeed, Mach number, dynamic pressure, normal acceleration, and wing sweep position. Flight test structural loads data were obtained for loads in both the wing box and the wing root. Data from uniformly deflected flaps were compared with data from flaps in the MLC configuration where the outboard segment of three flap segments was deflected downward less than the two inboard segments. The changes in the shear loads in the forward wing spar and at the roots of the stabilators also are presented. The camber control system automatically reconfigures the flaps through varied flight conditions. Configurations having both moderate and full trailing-edge flap deflection were tested. Flight test data were collected at Mach numbers of 0.6, 0.7, 0.8, and 0.9 and dynamic pressures of 300, 450, 600, and 800 lb/ft ² . The Reynolds numbers for these flight conditions ranged from 26×10^6 to 54×10^6 at the mean aerodynamic chord. Load factor increases of up to 1.0 g achieved with no increase in wing root bending moment with the MLC flap configuration.				
14. SUBJECT TERMS Load alleviation; Load distribution; Maneuver load control; Variable camber; Wing bending moment				15. NUMBER OF PAGES 32
				16. PRICE CODE A03
17. SECURITY CLASSIFICATION OF REPORT Unclassified (ITAR)		18. SECURITY CLASSIFICATION OF THIS PAGE Unclassified		19. SECURITY CLASSIFICATION OF ABSTRACT
20. LIMITATION OF ABSTRACT				

National Aeronautics and
Space Administration
Code JTT
Washington, D.C.
20546-0001
Official Business
Penalty for Private Use, \$300



3 1176 01409 6078

SPECIAL FOURTH-CLASS RATE
POSTAGE AND FEES PAID
NASA
PERMIT No. G27



POSTMASTER: If Undeliverable (Section 158
Postal Manual) Do Not Return
